

## Symmetric instability of monsoon flows

By V. KRISHNAKUMAR<sup>1\*</sup> and K.-M. LAU, *Climate and Radiation Branch, Laboratory for Atmospheres, NASA/Goddard Space Flight Center, Greenbelt, Maryland 20771, USA*

(Manuscript received 29 January 1996; in final form 30 August 1996)

### ABSTRACT

Using a zonally symmetric multi-level moist linear model, we have examined the possibility of symmetric instability in the monsoon region. Stability analyses with a zonally symmetric model using monthly ECMWF (Jan–Dec) zonal basic flows revealed both unstable as well as neutral modes. In the absence of cumulus heating, the linear stability of the monsoon flow changes dramatically with the emergence of many unstable modes in the month of May and lasting through August; whereas with the inclusion of cumulus heating unstable modes appear early in April with substantially enhanced growth rates. This onset of instability of the May basic state may signal the abrupt transition of the south Asian meridional monsoon circulation. The abrupt nature of the monsoon transitions was also clearly seen in the ECMWF 5-day mean meridional circulation in the South Asian monsoon region. The most unstable modes have doubling time of about 1 to 2 days. The amplitude structure of these unstable modes were mainly confined to the equatorial regions. The growth rates and the amplitude structure of the most unstable modes agree reasonably with the corresponding growth rate and structure of the meridional monsoon cell during the monsoon transition.

### 1. Introduction

Symmetric instability (SI), of zonal flow with both vertical and horizontal shear in the equatorial region has been well documented in the literature. SI in rotating fluids arises from an imbalance of pressure gradient and centrifugal (Coriolis) forces when the absolute value of angular momentum decreases with radius. Theoretical concepts of SI have been advanced by Kuo (1954), Eliassen (1952), Ooyama (1966), Stone (1966), Hoskins (1974), Emanuel (1979), Bennetts and Hoskins (1979) and Xu (1986). A detailed review with a historical perspective of inertial instability has been provided by Emanuel (1979). Charney (1973) showed that a basic state of the type  $u = u(y, z)$  on a  $\beta$ -plane is unstable to zonally symmetric

disturbances if  $fP < 0$  somewhere, where  $f$  is the Coriolis parameter and  $P$  is the Ertel potential vorticity of the basic state.

The importance of SI and its relevance in explaining different atmospheric phenomena have been recognized 2 or 3 decades ago. Some noteworthy studies of SI and its various applications are by Hoskins (1974), Bennetts and Hoskins (1979), Emanuel (1979), Dunkerton (1981, 1993), Boyd and Christidis (1982), Schubert and Hack (1982), Stevens (1983), Sun (1984), Stevens and Ciesielski (1986) and Zhang and Cho (1995). Emanuel (1979) studied the possible connection between inertial instability of the zonal flow and the middle latitude mesoscale circulation. The importance of conditional symmetric instability in the formation of frontal rainbands was first proposed by Bennetts and Hoskins (1979). Dunkerton (1981) investigated zonally symmetric linear perturbations on a zonally balanced flow with constant horizontal shear and static stability and

<sup>1</sup> Corresponding author.

\* Applied Research Corporation.  
e-mail: kishku@climate.gsfc.nasa.gov

found that in the absence of diffusion, the fastest growing mode was zonally symmetric at infinite vertical wavenumber. More recently, Dunkerton (1993) studied the inertial instability of zonally nonuniform, nonparallel flow near the equator. Schubert and Hack (1982) pointed out the important role of inertial stability in the rapid growth and development of cyclones. Stevens (1983) investigated the possibility of the equatorial SI of the mean flow in the troposphere with horizontal shear in the presence of Rayleigh friction and Newtonian cooling. In a follow up study, Stevens and Ciesielski (1986) investigated both symmetric and asymmetric instabilities for horizontally sheared flow away from the equator. Sun (1984) studied the formation and evolution of the rainbands along the Baiu front over Eastern Asia and squall lines over the eastern part of the United States.

The importance and relevance of SI in explaining various phenomena during the Asian summer monsoon has not been adequately or fully explored. Young (1981) showed that during MONEX (MONsoon EXperiment), data over the Indian Ocean region indicated the possibility of existence of inertial instability between equator to around  $10^{\circ}\text{N}$ . His computations for ( $40^{\circ}\text{S}$ – $20^{\circ}\text{N}$  and  $3^{\circ}\text{E}$ – $90^{\circ}\text{E}$ ) region showed that the possibility of inertial instability exists between the zero-line of absolute vorticity (around  $10^{\circ}\text{N}$ ) and the equator. Krishnakumar and Keshavamurty (1993) examined the possibility of SI of monsoon zonal flows during July incorporating moist convection. In the dry model as well as moist model they obtained both unstable and neutral modes with periods of oscillation around 1 to 5 days. Lau and Li (1984) and Lau et al. (1988) noted abrupt transitions in monsoon rainfall over the East Asian monsoon region starting in May and that the movement of the East Asian monsoon rainfall band appears to jump between stationary positions from lower latitudes to higher latitudes on short time scales. For a detailed review of East Asian summer monsoon rainfall transition and its impact on global climate fluctuations the readers are referred to Lau (1992). More recently, Lau and Yang (1996) investigated the onset, abrupt transitions and development of the summer monsoon system using output from a 10-year integration with the Goddard Laboratory for Atmospheres atmospheric (GLA) General

Circulation Model (GCM). They found that during the month of May there was an abrupt transition of monsoon rainfall as well as large scale atmospheric circulation in the monsoon region which may suggest the possible role of SI. Thus observational and modelling studies confirm sudden transitional features of monsoon rainfall and large scale circulation starting from the month of May. Another plausible mechanism is the sensitivity of the zonally symmetric flow to prescribed thermal forcing. Plumb and Hou (1992) studied the response of a zonally symmetric atmosphere to a prescribed thermal forcing located in the subtropics and found two distinct types of responses: (i) A steady state of thermal equilibrium with no meridional flow is obtained below a threshold forcing and (ii) Steady thermal equilibrium state breaks down and strong meridional circulation is predicted at the threshold forcing. Since their model has not considered the effect of latent heating and its associated feedback processes, its applicability in explaining monsoon onset is not very clear. One of the principal aims of this study is to examine the possibility of SI in the monsoon region and its possible role in monsoon transition using a set of zonally symmetric equations. We have conducted comprehensive linear stability analyses with a multi-level zonally symmetric model using the European Centre for Medium Range Weather Forecasts (ECMWF) basic flows of January to December incorporating a highly simplified parameterization of cumulus heating. As there is considerable amount of zonal symmetry in the monsoon region (ITCZ cloud zone), i.e., the zonal scale of the ITCZ is much larger than the meridional scale, zonally symmetric models may be a reasonable first approximation. Zonally symmetric models in studying symmetric circulations have been used by many studies (Charney, 1973; Schneider and Lindzen, 1977; Held and Hou, 1980; Goswami et al., 1984; Keshavamurty et al., 1986; Plumb and Hou, 1992). In further (model) studies the inclusion of longitudinal dependence in the basic equation is clearly needed.

In Section 2 of this paper, we describe in detail the multi-level zonally symmetric model. This section also discusses the type of cumulus heating used in this study and the method of solution. Section 3 gives the details of the data and observations used in the calculations. Section 4 presents

a detailed discussion on the zonally symmetric eigenmodes with and without interactive heating. Discussion and conclusions are provided in Section 5.

## 2. Governing equations

### 2.1. The model

A 10-level model in the vertical and a latitudinal domain of 42°S–42°N with 2° resolution have been chosen for the stability analysis. The model used for this analysis is a zonally symmetric primitive equation model and is essentially equivalent to that used by Krishnakumar and Keshavamurty (1993). The reason for choosing 10 vertical levels with a large latitudinal domain has been purely due to need to limit the larger computer memory requirements because of larger sizes of the matrices. The use of 10-levels in the vertical may just be adequate for this study. We are currently investigating this problem with a comprehensive model having a higher vertical resolution incorporating more complex basic states. The governing equations are the  $x$ - and  $y$ -momentum equations, the continuity equation and the thermodynamic energy equation in  $(x, y, p)$  co-ordinates. We consider the climatological monthly mean ECMWF basic flows  $U(y, p)$  in the longitude band 60°E–90°E which is representative of the South Asian summer monsoon region. Zonally symmetric perturbations are considered. The linearized set of equations around the mean zonal basic state are given by

$$\frac{\partial u'}{\partial t} + \left( \frac{\partial U}{\partial y} - f \right) v' + \omega' \frac{\partial U}{\partial p} = 0, \quad (1)$$

$$\frac{\partial v'}{\partial t} + f u' + \frac{\partial \phi'}{\partial y} = 0, \quad (2)$$

$$\frac{\partial}{\partial t} \left( \frac{\partial \phi'}{\partial p} \right) - v' f \frac{\partial U}{\partial p} + \sigma \omega' = - \frac{R}{C_p p} \dot{Q}', \quad (3)$$

$$\frac{\partial v'}{\partial y} + \frac{\partial \omega'}{\partial p} = 0, \quad (4)$$

where eqs. (1), (2) are the  $x$  and  $y$  component of the momentum equations, (3) is the thermodynamic energy equation and (4) is the continuity equation. In eqs. (1) to (4)  $u'$ ,  $v'$ ,  $\omega'$  are the perturbation eastward, northward and vertical velocities respectively,  $f$  is the Coriolis parameter,  $\phi'$

is the perturbation geopotential,  $R$  and  $C_p$  are the specific gas constant and the specific heat at constant pressure,  $\dot{Q}'$  is the rate of nonadiabatic heating and  $\sigma$  is the static stability.

### 2.2. Cumulus heating

A simple scheme by Lau and Peng (1987) of parameterizing the effects of cumulus heating is included. It parameterizes the rate of cumulus heating by

$$\frac{\dot{Q}'}{C_p} = -mrLq_{\text{sat}}(T_L)\eta(p) \frac{\Delta p}{C_p p_0} \left( \frac{\partial v'_L}{\partial y} \right), \quad (5)$$

where  $m$  is the moisture availability factor;  $r$  the relative humidity;  $L$  the latent heat of condensation;  $q_{\text{sat}}(T_L)$  the saturation specific humidity at temperature  $T$ , the suffix  $L$  meaning the values defined at the lowest model layer;  $p_0$  surface pressure;  $\Delta p$  is the vertical grid length. Here  $\partial v'_L / \partial y$  is the divergence at the model level (referred to by the suffix  $L$ ). For linear analysis, we have used only the simple wave-CISK type of heating and not the positive-only wave-CISK originally proposed by Lau and Peng (1987). Here  $\eta(p)$  is the normalized heating function whose vertical integral is unity. In the above set of equations, we have assumed that the mean zonal basic state  $U(y, p)$  is in thermal wind balance with the basic geopotential field  $\bar{\Phi}(y, p)$ . We have explicitly calculated the thermal wind balance conditions from the ECMWF monthly mean cross-sections of zonal wind, geopotential and temperature fields and found that the basic state flow is in reasonably good thermal wind balance overall.

The thermodynamic energy equation with the inclusion of moisture becomes

$$\frac{\partial}{\partial t} \left( \frac{\partial \phi'}{\partial p} \right) - v' f \frac{\partial U}{\partial p} + \sigma \omega' = \frac{K}{p} \sin \left( \frac{\pi p}{p_0} \right) \frac{\partial v'_L}{\partial y}. \quad (6)$$

The constant  $K$  is given by

$$K = \frac{RmrLq\Delta p\mathcal{N}}{p_0 C_p}, \quad (7)$$

where  $\mathcal{N}$  is the normalization constant. A simple profile of the form  $\sin(\pi p/p_0)$  is used to represent the vertical distribution of heating which is quite consistent with the observed profiles for the monsoon and tropical areas. Geisler and Stevens (1982) showed that the tropical convective heating distri-

bution has the structure of the first baroclinic mode with a single maximum around 500 mb. Schaack et al. (1990) estimated the three-dimensional distribution of atmospheric heating over different parts of the globe from the ECMWF GWE Level IIIb data set. The vertical profiles of time-averaged heating for the summer months over the Asian monsoon region show maximum heating concentrated around 400 mb to 500 mb. This cumulus heating with its vertical structure can be considered as highly idealized. Earlier studies of SI (Sun, 1984) applied simple forms of wave-CISK heating to understand the formation and evolution of rainbands or the squall lines and obtained reasonable results. We have not considered the effect of cumulus mixing proposed by Schneider and Lindzen (1976). Omission of the cumulus friction effects in a simple wave-CISK type of heating formalism is likely to affect the structure of the unstable modes. Our object here is to gain a first order understanding of role of SI of the zonal monsoon flows in monsoon transition using a very simple parameterization of cumulus heating. The present results are clearly sensitive to the heating scheme. The common caveats of wave-CISK heating should be applicable here (Mak, 1981). In our subsequent studies we plan to use a detailed model including a realistic parameterization of slantwise convection and study this problem with an initial value approach.

Since the continuity equation takes a simple form, the meridional circulation components ( $v'$  and  $\omega'$ ) can be expressed in terms of single streamfunction  $\psi'$  such that  $v' = -\partial\psi'/\partial p$  and  $\omega' = \partial\psi'/\partial y$  from (4). Eliminating  $u'$  between eqs. (1) and (2) we get

$$\frac{\partial^2 v'}{\partial t^2} + \frac{\partial}{\partial t} \left( \frac{\partial \phi'}{\partial y} \right) - f \left( \frac{\partial U}{\partial y} - f \right) v' - f \omega' \frac{\partial U}{\partial p} = 0. \tag{8}$$

Eliminating  $\phi'$  between eqs. (6) and (8) and substituting for  $v'$  and  $\omega'$  in terms of  $\psi'$ , we finally get

$$\begin{aligned} & \left\{ -\frac{\partial^2}{\partial t^2} - f \left( f - \frac{\partial U}{\partial y} \right) \right\} \frac{\partial^2 \psi'}{\partial p^2} - \beta \frac{\partial U}{\partial p} \frac{\partial \psi'}{\partial p} \\ & - 2f \frac{\partial U}{\partial p} \frac{\partial}{\partial p} \left( \frac{\partial \psi'}{\partial y} \right) - f \frac{\partial^2 U}{\partial p^2} \frac{\partial \psi'}{\partial y} - \sigma \frac{\partial^2 \psi'}{\partial y^2} \\ & - \frac{K}{p} \sin \left( \frac{\pi p}{p_0} \right) \frac{\partial^2}{\partial y^2} \left( \frac{\partial \psi'}{\partial p} \right)_L = 0. \end{aligned} \tag{9}$$

We assume solutions of the form

$$\psi' = \Psi(y, p) e^{i\nu t}, \tag{10}$$

where  $\Psi(y, p)$  is the perturbation streamfunction amplitude and  $\nu$  is the frequency of oscillation. Substituting (10) into (9) we get

$$\begin{aligned} & \left\{ \nu^2 - f \left( f - \frac{\partial U}{\partial y} \right) \right\} \frac{\partial^2 \Psi}{\partial p^2} - \beta \frac{\partial U}{\partial p} \frac{\partial \Psi}{\partial p} \\ & - 2f \frac{\partial U}{\partial p} \frac{\partial}{\partial p} \left( \frac{\partial \Psi}{\partial y} \right) - f \frac{\partial^2 U}{\partial p^2} \frac{\partial \Psi}{\partial y} - \sigma \frac{\partial^2 \Psi}{\partial y^2} \\ & - \frac{K}{p} \sin \left( \frac{\pi p}{p_0} \right) \frac{\partial^2}{\partial y^2} \left( \frac{\partial \Psi}{\partial p} \right)_L = 0. \end{aligned} \tag{11}$$

Our approach is to solve (11) for  $\nu$  the frequency and  $\Psi$  to get the zonally symmetric eigenmodes and its ( $y$ - $p$ ) structure. Since (11) is non-separable in its  $y$  and  $p$  dependence, we have to employ numerical methods for solution and the computational details are given in the Appendix.

### 3. Data and observations

#### 3.1. Basic state

The climatological zonal basic flows for January to December have been taken from the 9-year (1980–88) ECMWF analyses. A symmetric stability analysis was performed for the basic flows obtained by zonal averaging in the longitude band 60°E–90°E. Fig. 1 shows the ECMWF climatological latitude-pressure section of the zonal component of wind averaged between 60°E–90°E for January to December from 40°S to 40°N. The zonal wind distribution in both hemispheres for all months is dominated by strong westerly jets with maximum velocities around 40 m s<sup>-1</sup> and 30 m s<sup>-1</sup> in the northern winter and summer hemispheres respectively except for April and October where the westerly jets have approximately the same strength in both hemispheres. The monsoonal westerlies in the lower troposphere emerge in May. The zonal flows during June to September are dominated by a strong westerly current in the lower troposphere between 5°S to 25°N up to 500 mb with a core of about 10 m s<sup>-1</sup> centered around 8°N to 13°N at 850 mb and a strong easterly flow in the upper troposphere with strengths exceeding 25 m s<sup>-1</sup> centered around 10°N to 20°N at 100 mb. Mean static stability ( $\sigma$ )



for the above longitude band was computed from the geopotential ( $\Phi$ ) field for the months January to December and the monthly distributions were quite similar. The mean static stability profiles (not shown) indicate that the mean atmosphere is stable. As mentioned previously, the thermal wind balance conditions calculated from the monthly mean cross-sections of zonal wind, geopotential and temperature fields show reasonably good balance.

3.2. Stability criterion

In this section, we have examined the necessary condition for SI, i.e.,  $fP$  of the mean zonal flows (here, the mean flows of January to December) on an isentropic surface is negative somewhere in the fluid domain, where  $f$  is the Coriolis parameter and

$$P = -g \left\{ \frac{\partial U}{\partial p} \left( \frac{\partial \Theta}{\partial y} \right)_p + \left[ - \left( \frac{\partial U}{\partial y} \right)_p + f \right] \frac{\partial \Theta}{\partial p} \right\}, \tag{12}$$

is the Ertel potential vorticity of the basic state. The subscript  $p$  denotes that derivatives are taken on constant pressure surfaces. Calculations of  $fP$  performed on isobaric surfaces using the ECMWF climatological profiles of zonal wind ( $U$ ) and potential temperature ( $\Theta$ ) for January to December reveal negative regions, thus satisfying the necessary condition for SI. Figs. 2a, b show the latitude-pressure cross sections of potential vorticity of the mean flows in the longitudinal band 60°E–90°E for the months January and July respectively. The key features in the profiles of potential vorticity are the regions of negative (positive) potential vorticity in the northern (southern) hemisphere. It is interesting to note that the zero line of the potential vorticity shifts 5°–6° into the summer hemisphere in the equatorial lower troposphere as evident in Fig. 2. Region of negative (positive) potential vorticity is evident in the upper troposphere but is most pronounced around 200 mb between 10°N to 20°N (10°S to 20°S) as seen in Fig. 2a (Fig. 2b). Our calculations revealed that the necessary condition for SI is satisfied practically for all summer months between equator to around 6°N.

We have also examined the necessary criterion for (moist) symmetric instability, i.e.,  $fP_m$  of the mean zonal flows starting from January to

December on an isentropic surface is negative somewhere in the fluid domain, where  $P_m$ , the moist potential vorticity (MPV) is same as (12) but with  $\Theta$  replaced by  $\Theta_e$  the equivalent potential temperature. Calculations of  $fP_m$  performed on isobaric surfaces using the ECMWF climatological profiles of zonal wind ( $U$ ) and equivalent potential temperature ( $\Theta_e$ , derived from specific humidity and temperature fields) for January to December reveal negative regions in areas where convective instability (CI) is absent, satisfying the possibility of SI in a moist atmosphere (not shown). In the absence of CI, negative MPV exists from 700 mb to 300 mb between equator to around 10°N for the summer months. The upper tropospheric distribution of MPV is very similar to dry potential vorticity fields calculated for all months (Fig. 2).

3.3. Monsoon transitions

Abrupt transitions in large-scale circulations and rainfall during the “Mei-Yu” regime (mid-May to mid-June) over the East Asian monsoon region were noted by Lau and Li (1984). Associated with this transition, an abrupt northward progression of the low-level westerlies and upper-level easterlies to the foothills of the Himalayas over the South Asian monsoon region takes place. Similar abrupt northward shift of the upper level westerlies over eastern China and Japan is also seen. The abrupt nature of the monsoon transitions was also simulated in the GLA GCM (Lau and Yang, 1996). Fig. 3 shows the ECMWF 5-day mean latitude-pressure section of the zonal wind and meridional circulation in the longitudinal band 60°E–90°E from mid May to mid June. The meridional overturning of the monsoon begins to develop during May 21–25 at around 5°N. By 1–5 June a fully developed monsoon cell with strong ascending motion is found around 15°N indicating the onset of South Asian summer monsoon. The abrupt transition of the axis of the vertical motion of the monsoon cell from equatorial latitudes to northern latitudes 10°N–15°N happens around 1–5 June. The characteristic features of monsoon onset such as the strengthening of the low-level westerlies and upper-level easterlies are also clearly seen. One of our principal aims in this study, is to understand the dynamical reasons for this abrupt transition.

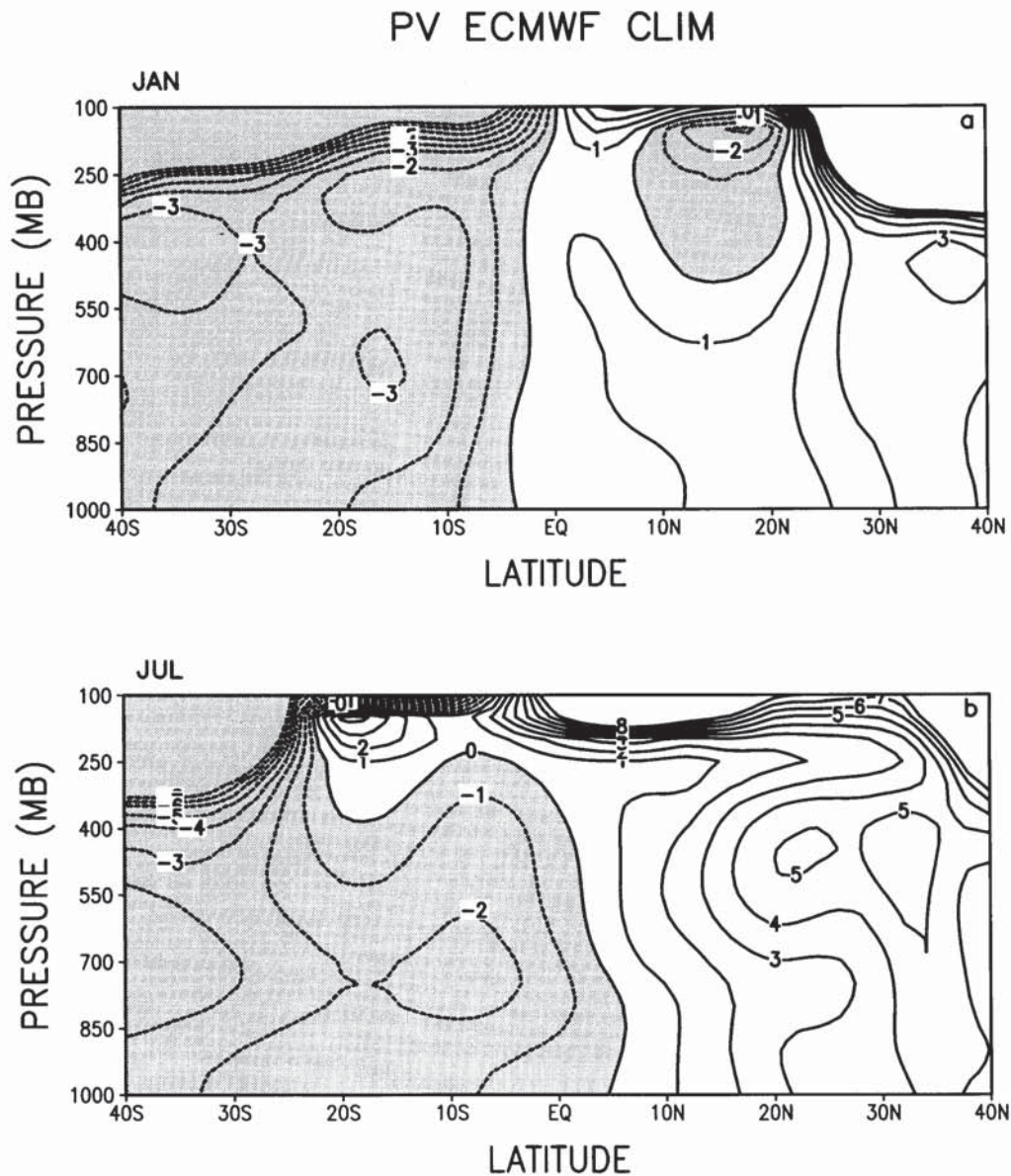


Fig. 2. Latitude-pressure cross section of potential vorticity (PV) calculated using ECMWF climatological profiles of zonal wind and potential temperature between  $60^{\circ}\text{E}$ – $90^{\circ}\text{E}$  for (a) January and (b) July at intervals of  $10^{-7} \text{ K m}^2 \text{ kg}^{-1} \text{ s}^{-1}$ . Shaded areas denote negative values.

To focus on the monsoon transition, we have separately carried out stability analyses using the ECMWF pentad mean basic flows of May and June and the results are outlined in the next section.

#### 4. Zonally symmetric eigenmodes

We have conducted the stability analyses with and without cumulus heating. For both cases, unstable and neutral modes are obtained. In the

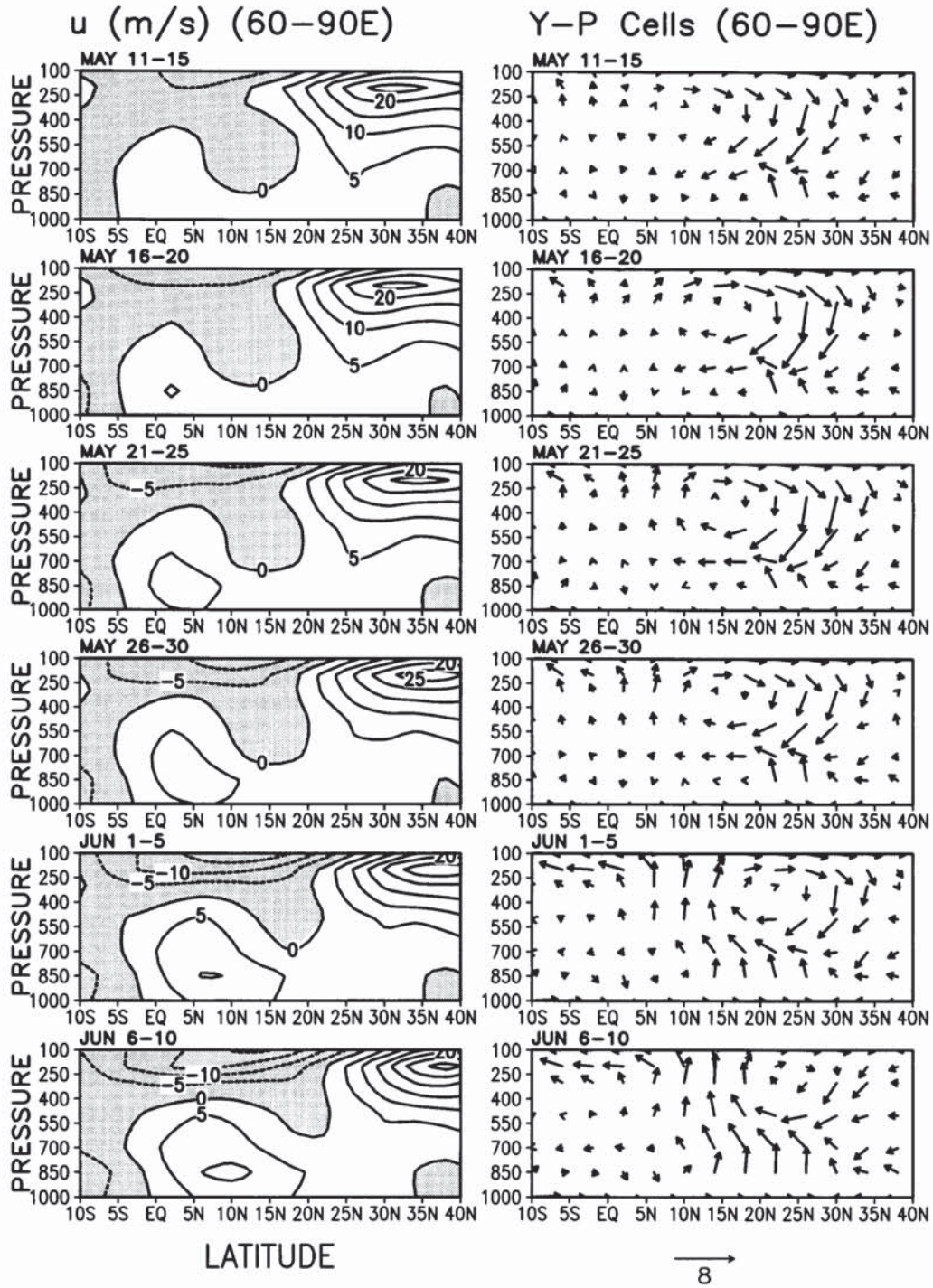


Fig. 3. Zonal wind ( $m s^{-1}$ ) and meridional circulation between  $60^{\circ}E-90^{\circ}E$  longitude band from ECMWF climatology. The vertical motion has been amplified by 100 times in the plots.

following sections, we discuss the results based on cases with and without incorporating cumulus heating.

#### 4.1. Growing modes

*4.1.1. No heating.* We have performed the stability analyses separately by considering basic flow of each month (starting from January to December) to investigate the behavior of zonally symmetric eigenmodes under the influence of basic flows. The normal modes of the system were first determined for the case of no heating, no dissipation and a resting basic state. We found two sets of fast oscillating inertia-gravity modes with periods 0.3 days to 0.9 days and slowly oscillating modes with periods 1 to 5 days similar to the analytical results of Matsuno (1966). The next case includes the zonal mean basic flows (starting from January to December) without cumulus heating. Fig. 4a (dashed line marked NH) shows the growth rate, measured in doubling time  $\tau_d = \ln 2/\nu_i$  of the most unstable eigenmodes of the zonally symmetric model as a function of all calendar months (starting from January to December). Only the doubling times for the most unstable modes with period of oscillation greater than 1 day are shown. Fast oscillating inertia gravity modes with periods of oscillation less than one day were separated from this diagram based on the spatial structures of eigenvectors. One of the key features to note is that without cumulus heating the most unstable modes begin to emerge in the month of May and last through August. The presence of unstable modes found in the summer monsoon months starting from May to August implies that the zonal flows in the monsoon region exhibit SI. Fig. 5a shows the spectrum of all the unstable modes (period versus doubling time) for the month of May with (WH) and without (NH) cumulus heating. In the case of no heating, the most unstable mode has a distinctly larger growth rate than all the other growing modes. It is interesting to note that the linear stability of the monsoon flow changes dramatically in the month of May and this onset of instability of the basic state occurring in May may be associated with the observed abrupt transition of the south Asian meridional monsoon circulation. The most unstable modes have period of oscillation in the range of 1 to 2 days and doubling time around

2 days. An abrupt transition in the development of monsoon during May was seen in observations (Lau and Li, 1984) as well as reproduced in a GCM simulation (Lau and Yang, 1996).

In order to focus the monsoon transition which occurs in a short time scale we performed the stability analyses without the inclusion of cumulus heating using the ECMWF pentad mean zonal flows starting from 1–5 May to 26–30 June thereby treating the basic state significantly more carefully. The growth rate diagram of the most unstable eigenmodes plotted as a function of time for all the 12 pentads starting from 1–5 May to 26–30 June, as shown in Fig. 4b (dashed line marked NH), reveals higher growth rates (smaller doubling times) in the pentads (6 and 7) corresponding to 26–30 May and 1–5 June respectively which agrees with the time of occurrence of the monsoon transition seen in ECMWF 5-day mean climatology (see Fig. 3). Fig. 5b shows the spectrum of all the unstable modes as a function of period and doubling time for the pentad corresponding to 26–30 May with (WH) and without (NH) cumulus heating. There is also a sudden emergence of many unstable modes in the pentad 7. The sudden appearance of these unstable modes in 26–30 May is indicative of the onset of SI which may be responsible for the observed abrupt transition of the monsoon. Our calculations with the monthly mean basic flows also reveal that the onset of instability takes place in the month of May with doubling time of a couple of days and it may be argued that the SI of the mean May zonal flow may be a plausible explanation for the abrupt monsoon transition. Other mechanisms may also be at work as proposed by Plumb and Hou (1992).

Spatial structure of the most unstable modes in the months May to August show multi-cellular patterns of latitudinal dimension about  $10^\circ$  to  $15^\circ$  with varying intensities (not shown). The amplitudes are mainly distributed in the lower and middle tropospheres. In practice, the spatial structure of these modes may not be realized in nature for the large scale monsoon, because of the interaction with latent heating and excitation of coupled convective heating/circulation modes. The modal structure during the months May to August may give an indication where the real unstable modes tend to occur. The deficiencies of the modal eigenstructures may also be attributed to the

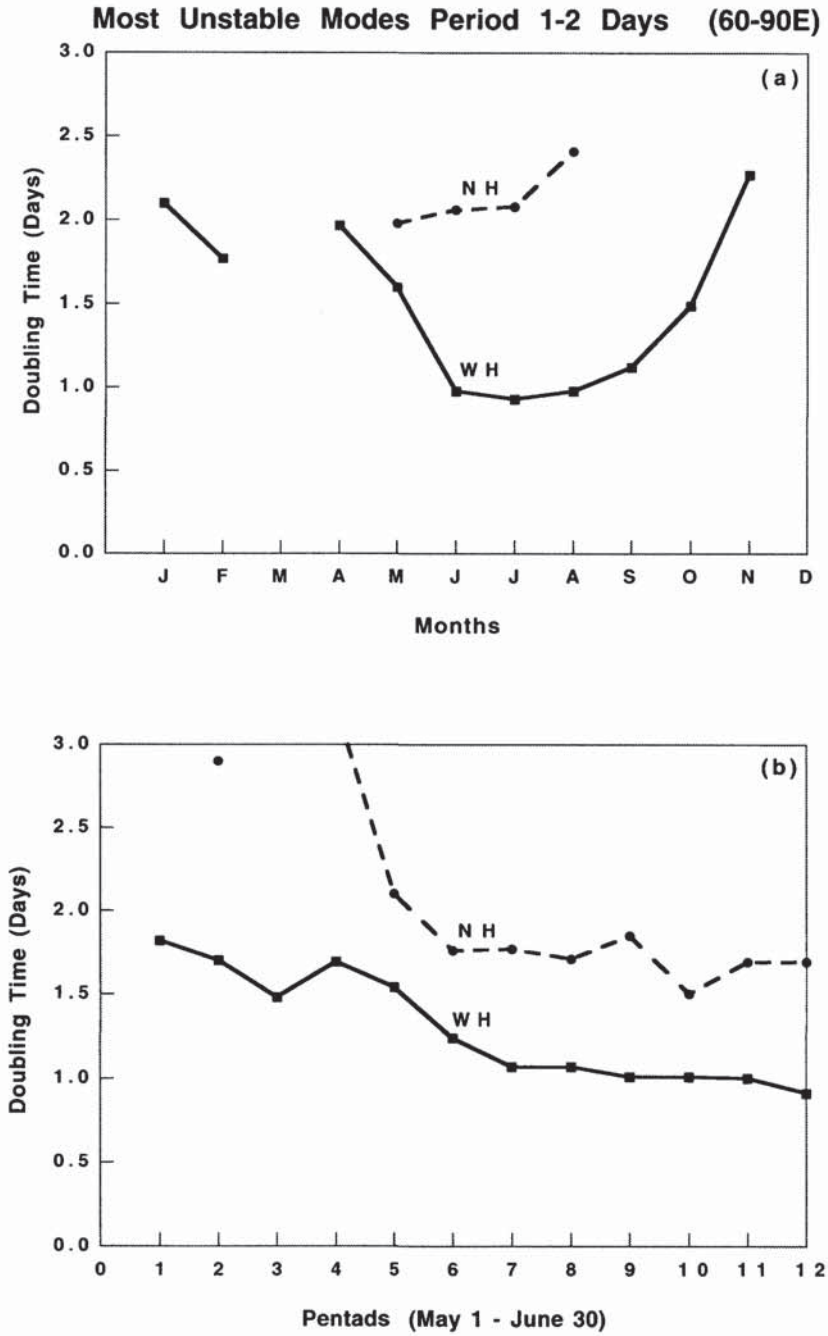


Fig. 4. Doubling time as a function of time for the most unstable modes with no cumulus heating (NH) and with cumulus heating (WH) calculated (a) using the mean monthly basic flows from January to December and the two curves dashed line (NH) is with no cumulus heating and the solid line (WH) is with cumulus heating (b) As in Fig. 4(a) but using the pentad mean basic flows from 1-5 May to 26-30 June. Modes with period > 1 day are plotted.

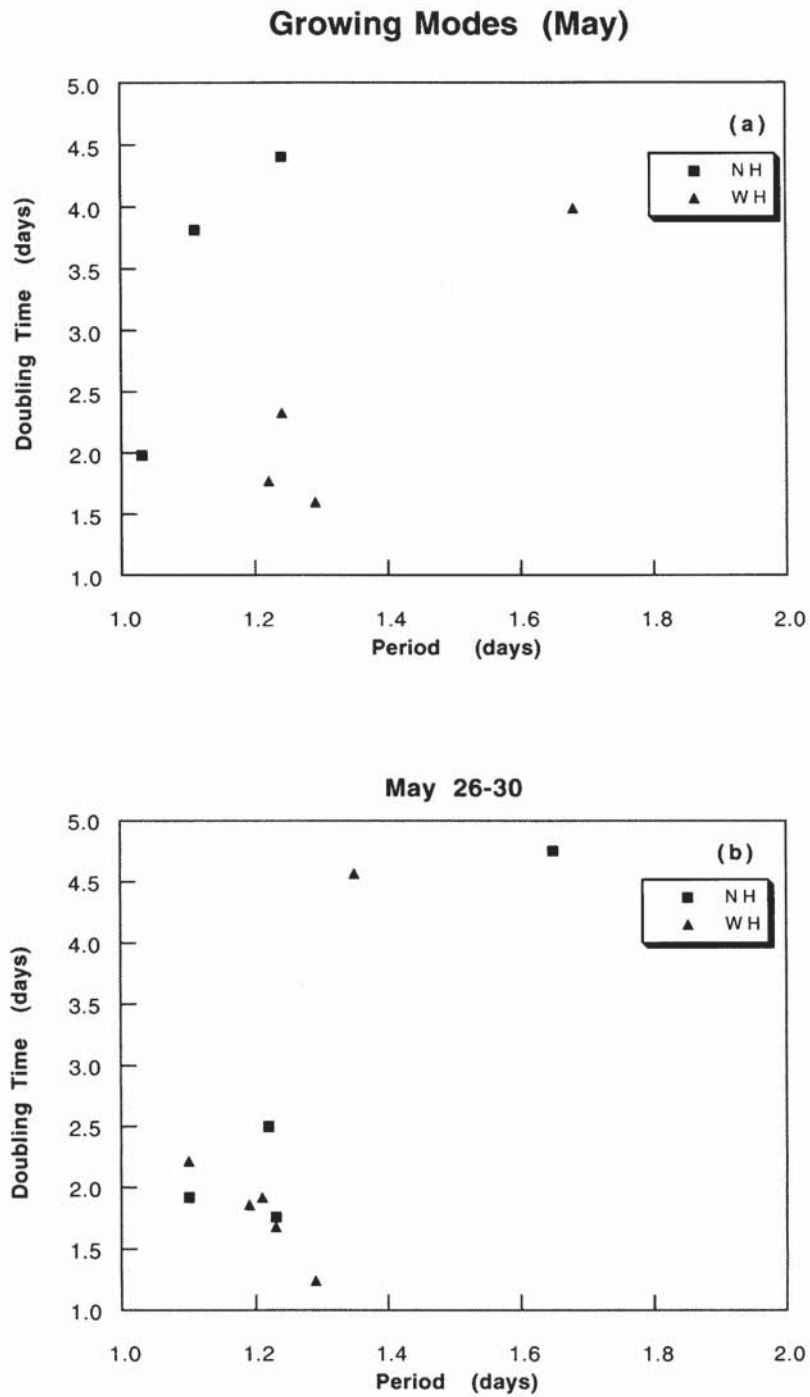


Fig. 5. Period (days) versus doubling time (days) of growing modes with no cumulus heating (NH) and with cumulus heating (WH) calculated using (a) the monthly mean basic flow for May (b) the pentad mean basic flow for 26–30 May.

omission of the Hadley basic state as well as the lack of a realistic cumulus parameterization.

In nature, during the onset and advancing phase of the monsoon, it is well-known that the ITCZ and its associated cloud bands move northwards from the equator and hence cumulus heating may play a dominant role on the structure of zonally symmetric eigenmodes. Next, we examine the effect of cumulus heating on the overall behavior of these modes.

*4.1.2. With heating.* We have used a simple scheme of including the effects of cumulus heating proposed by Lau and Peng (1987) to determine the role of cumulus heating on the growth and structure of the zonally symmetric eigenmodes. Fig. 4a (solid line marked WH) shows the doubling time of the most unstable eigenmodes as a function of time with periods of oscillation greater than 1 day for all months. We have separated fast oscillating inertia gravity modes with periods of oscillation less than one day based on their spatial structures of eigenvectors as in the previous case. One of the discerning features is that in the presence of cumulus heating the unstable modes begin to emerge in April and last through October and their growth rates are substantially enhanced. A large number of unstable modes with higher growth rates were found in the summer months May, June and July. A comparison of the curves labelled WH and NH in Fig. 4a reveals that in the presence of cumulus heating the unstable modes begin to appear early in April rather than in May. Also it may be noted that the doubling times of the most unstable modes are reduced to half or growth rates enhanced by a factor of two compared to the doubling times without heating. We performed a set of calculations with varying moisture availability factor in the Lau and Peng (1987) scheme using the basic flows of April to see the sensitivity of unstable modes to cumulus heating. Our calculations reveal that these modes originated only when cumulus heating was included in the model. The sudden appearance of many unstable modes with large growth rates clearly seen in May, as revealed in the spectrum of the growing modes with heating (see Fig. 5a modes marked WH), lasting through the monsoon months June to September, may be a manifestation of monsoon transition. Fig. 4b (solid line marked WH) shows the growth rate diagram of the most

unstable eigenmodes with cumulus heating plotted as a function of time for all the 12 pentads starting from 1–5 May to 26–30 June. The interesting feature is that the most unstable modes found in the pentads (6 and 7) corresponding to 26–30 May (see Fig. 5b modes marked WH for the spectrum of growing modes) and 1–5 June respectively preferentially grow faster than the modes found before the transition (pentads 4 and 5). Plumb and Hou (1992) showed that when the off-equatorial thermal forcing exceeds a critical value steady thermal equilibrium state breaks down and angular momentum conserving circulations set in. The dramatic strengthening of the low-level westerlies and upper-level easterlies seen during the monsoon transition period as illustrated in Fig. 3 may have a possible connection with the critical thermal forcing in the model of Plumb and Hou (1992) and this needs to be investigated further. However, their model did not consider the effect of latent heating and therefore its applicability in explaining monsoon transition is not very clear. They did not also address the issue of SI of the mean flows and our results may be viewed as complimentary.

The eigenstructure of the growing modes obtained with the inclusion of cumulus heating for the months May to July is discussed next. We first discuss the structure of the unstable modes seen in May. Figs. 6a, b show latitude-pressure cross sections of the real and imaginary parts of streamfunction of the most unstable mode obtained from Fig. 4b (solid curve WH) corresponding to May 26–30 (pentad 6) with an oscillatory part with period 1.28 days and doubling time 1.24 days. Figs. 6c, d show similar cross sections of the most unstable mode obtained from Fig. 4a (solid curve WH) corresponding to the mean May conditions with a period of oscillation 1.29 days and doubling time 1.60 days. The meridional structure of the streamfunction field of the most unstable mode is characterized by four circulation patterns with maxima located around 15°S, 5°S, 5°N and 20°N (Fig. 6a). The shaded regions in Figs. 6a, b indicate the calculated vertical motions ( $\omega$ ). Maximum vertical motions are located around 10°S and 10°N as shown. Such bimodal structures of ITCZ on the two sides of the equator are also observed over the Asian summer monsoon region during the onset phase (Sikka and Gadgil, 1980). The meridional structure of the streamfunction field of the most unstable mode corresponding to

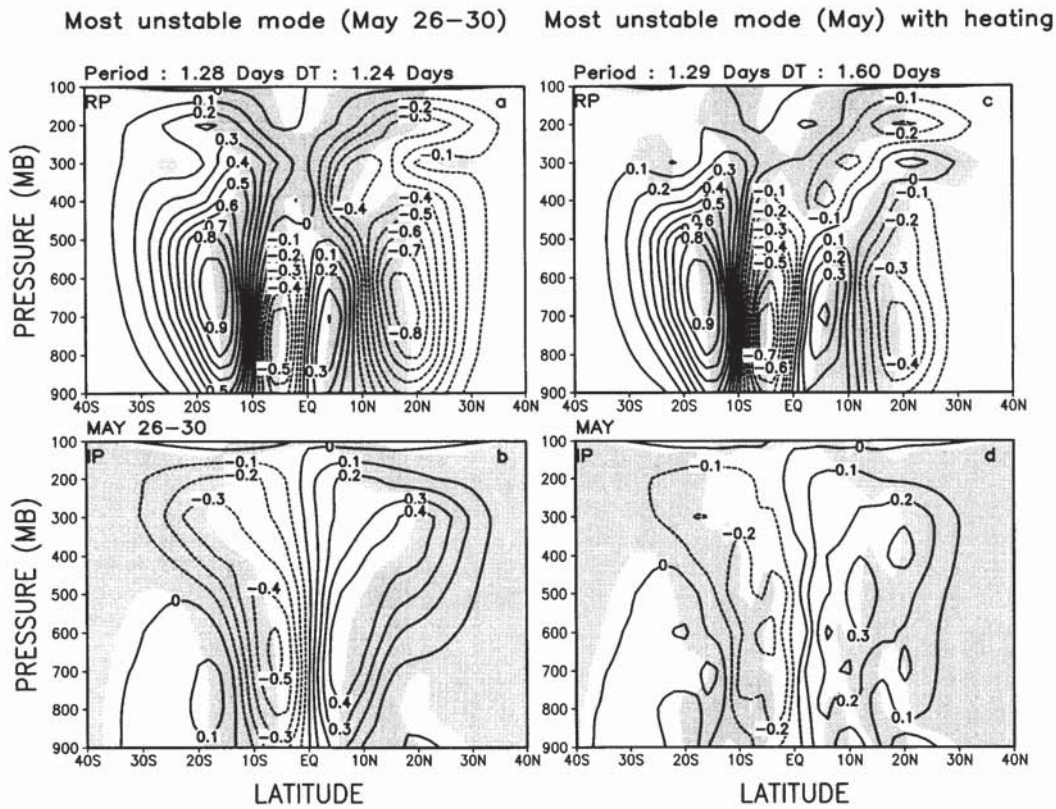


Fig. 6. Latitude-pressure cross sections of the real parts of normalized streamfunction of the most unstable modes with cumulus heating obtained from (a) Fig. 4b (the curve marked WH) for the pentad mean basic flows and (c) Fig. 4a (the curve marked WH) for the mean monthly basic flows. The corresponding imaginary parts of normalized streamfunction of the most unstable modes with cumulus heating obtained from (b) Fig. 4b (WH) and (d) Fig. 4a (WH). Shadings indicate regions of vertical motions.

mean May conditions (Figs. 6c, d) shows similar structures as in Figs. 6a, b except that the circulations located in the southern hemisphere are much stronger than that of the northern hemispheric circulations. Fig. 7 shows latitude-pressure cross sections of the real and imaginary parts of streamfunction of unstable modes for June with period of oscillation 1.28 days and doubling time 0.98 days (Figs. 7a, b) and July with period of oscillation 1.26 days and doubling time 0.93 days (Figs. 7c, d) obtained from Fig. 4a (solid curve WH). The streamfunction distribution is characterized by two circulation patterns in both hemispheres with centers located around  $15^{\circ}\text{S}$  and  $15^{\circ}\text{N}$  in both hemispheres (Figs. 7a, c). The resulting vertical  $p$ -velocity fields (shaded regions) indicate strong vertical motions in the equatorial

region from  $12^{\circ}\text{S}$  to  $8^{\circ}\text{N}$  with maximum located in the middle troposphere. The vertical structure of the heating modes has greater vertical extension compared to that of modes without heating (figures not shown). It may be noted that the chosen vertical heating distribution in our cumulus parameterization scheme has a maximum at 500 mb and quite consistently, the spatial pattern of the growing modes with heating also has maximum in the middle troposphere. The asymmetric distribution of streamfunction is also seen in the imaginary parts during June (Fig. 7b) and July (Fig. 7d). The streamfunction distribution corresponding to the most unstable mode of June (Figs. 7a, b) at different phase angles from 0 to  $\pi/2$  (not shown) reveals changes in the structure from two circulation patterns with deep vertical struc-

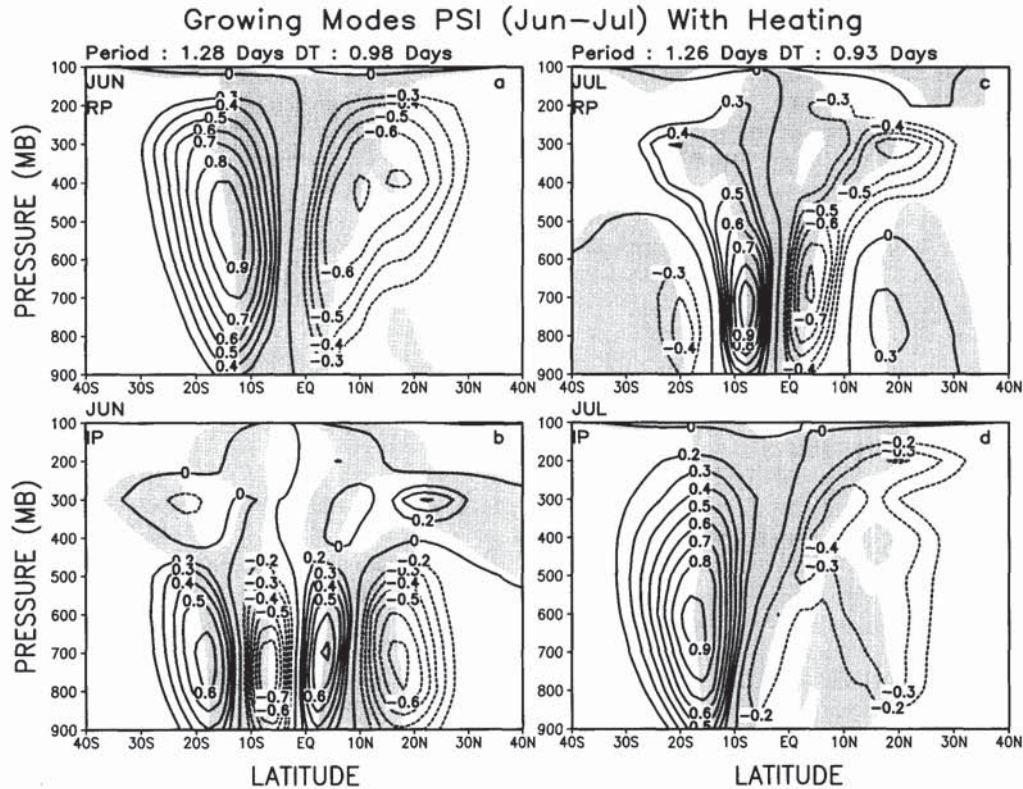


Fig. 7. Latitude-pressure cross sections of the real parts of normalized streamfunction of the most unstable modes with cumulus heating obtained from Fig. 4a (the curve marked WH) for the mean monthly basic flows of (a) June and (c) July. The corresponding imaginary parts of normalized streamfunction of the most unstable modes with cumulus heating for (b) June and (d) July. Shadings indicate regions of vertical motions.

tures (RP, Fig. 7a) exhibiting contraction in horizontal scale at the lower troposphere finally transforming to four circulation patterns with shallow vertical structures (IP, Fig. 7b). This seems to indicate that there is some coupling between the deep structure (due to cumulus heating) and shallow structure (due to inertial instability). It is interesting to note that the real part of the streamfunction field corresponding to the most unstable modes during the pentad May 26–30 as well as mean May basic flow (Figs. 6a, c respectively) shows double cell structure of ITCZ with ascending motions located on the two sides of the equator whereas during June (Figs. 7a, b), the circulation shows evolution between a single rising branch (ITCZ) vs a double ITCZ. The circulation becomes more intense during the peak monsoon month July as evident in Figs. 7c, d. The observed

circulation patterns during June and July show a dramatic strengthening of meridional basic state as well as convection. While the modal structure found during the transition month in May agrees fairly with the observed monsoon meridional cell, the meridional modal structures found in June and July differ significantly from the observed structures. This may be due to the absence of Hadley basic state in our calculations which may drastically affect our results especially for June and July.

We have also performed calculations with a higher horizontal resolution of 1° latitude to check the sensitivity of the most unstable modes and its *y-p* structure to horizontal resolution. The growth rate and eigen structure of the most unstable modes were not very sensitive to horizontal resolution.

The structure of zonally symmetric growing modes in the absence of heating as discussed in subsection 4.1.1, had multi-cellular patterns with very shallow vertical dimension and amplitudes centered away from the equator between  $10^{\circ}\text{N}$  to  $20^{\circ}\text{N}$  (not shown). In the presence of cumulus heating, the fast growing modes all have  $\Psi$  field distributed asymmetric to the equator as indicated in Figs. 7a, d and with vertical motions symmetric with respect to the equator with maximum at around 500 mb. Growing modes with shallow vertical structures similar to the case of no heating were found for the heating case also. However these shallow modes were all slowly growing. The above results indicate that in the presence of heating only asymmetric modes grow faster than other modes. The eigenstructure of the unstable modes found during May in the presence of cumulus heating agree fairly with the structure of the meridional cell during the monsoon transition time. However, the modal eigenstructures have significant discrepancies in intensity and the latitudinal position of the vertical motions as compared to the observed structures found during the monsoon transition. These may presumably be caused by the omission of the Hadley type meridional overturning in the basic state as well as the lack of a realistic cumulus parameterization scheme.

In order to investigate the role of basic flows and cumulus heating during the monsoon transition the stability analyses were carried out using the basic flows in the longitude band  $90^{\circ}\text{E}$  to  $120^{\circ}\text{E}$  which is representative of the East Asian summer monsoon region starting from January to December. The essential results during the summer monsoon months from this analyses are very similar to that of the analyses in the longitudinal band  $60^{\circ}\text{E}$  to  $90^{\circ}\text{E}$ . The mean summer monsoon flow in the presence of cumulus heating can effectively destabilize equatorial symmetric modes with largest growth rates found during the months May and June (not shown). One of the important differences between the  $90^{\circ}\text{E}$ – $120^{\circ}\text{E}$  and  $60^{\circ}\text{E}$ – $90^{\circ}\text{E}$  case is the appearance of growing modes during the winter months November to February in the former. The existence of growing modes during the winter regime may be related to winter monsoon large-scale mean circulation conditions over East and Southeast Asia (see Lau and Li, 1984). This needs further investigation

with a detailed model and is beyond the scope of the present study. Linear SI calculations using this model of the monthly mean basic zonal flow derived from the 10 year Atmospheric Model Intercomparison Project (AMIP) of the Goddard Laboratory for Atmospheres (GLA) general circulation model (GCM) in the longitude sector for East Asia ( $110^{\circ}\text{E}$ – $120^{\circ}\text{E}$ ) indicate that inherent instability for the monsoon flow is present in the basic flow in May before the monsoon circulation is fully developed (Lau and Yang, 1996). The overall results seem to suggest that moist SI exists, as revealed by the presence of many unstable modes, in late boreal spring over a much wider zone covering from  $60^{\circ}\text{E}$  to  $120^{\circ}\text{E}$ .

## 5. Discussion and conclusions

In this paper, we have examined the possibility of SI with a zonally symmetric multi-level model in the tropical (monsoon) region with a view to investigate the physical mechanisms governing the features of the abrupt transition of the monsoon meridional cell. We have conducted comprehensive linear stability analyses with the multi-level zonally symmetric model using climatological monthly basic flows derived from ECMWF analyses from January to December as well as ECMWF pentad mean zonal flows starting from 1–5 May to 26–30 June. A simple wave-CISK scheme for parameterizing the effects of cumulus heating was considered. Calculations were performed with and without the inclusion of cumulus heating. The key findings of this paper are:

Stability analyses performed in the absence of heating reveal that the most unstable modes were found in the month of May and last through August. The fastest growing modes occurred in the summer monsoon months from May to July. A well marked transition appears in May in the growth rate curve of the most unstable eigenmodes plotted against all months. Sudden appearance of many unstable modes was found in the pentads corresponding to 26–30 May which may be indicative of the transitional nature of the onset of the South Asian meridional monsoon circulation. The streamfunction amplitude distribution of the most unstable modes exhibit shallow vertical structures with maximum amplitudes between  $10^{\circ}\text{N}$  to  $20^{\circ}\text{N}$ .

In the presence of cumulus heating, the stability

analyses with the monthly basic flows reveal that the most unstable modes were found in April and last through October and their growth rates are also enhanced by a factor of two as compared to the growing modes without heating. Growing modes emerged in April only when cumulus heating was included. Stability analyses results during the summer monsoon months for the longitude sector 90°E–120°E are very similar to that of the analyses in the longitude sector 60°E–90°E. In the stability analyses with the pentad mean basic flows, many unstable modes with large growth rates were found in the pentads corresponding to 26–30 May and 1–5 June. The finding of the most unstable modes during May to June illustrate the transitional nature of the onset of south Asian monsoon. The streamfunction distribution of the most unstable modes in May is characterized by double cell structure with the resulting vertical motions located around 10°S and 10°N. Such bimodal structures of ITCZ on the two sides of the equator are also observed over the Asian summer monsoon region during the onset phase. The streamfunction distribution of the most unstable modes found during June and July is characterized by a single cell structure with the resulting vertical motions in the equatorial regions from 8°S to 8°N and has the structure of the first baroclinic mode consistent with the cumulus heating distribution maximum located at 500 mb. In the presence of cumulus heating, the asymmetric modes, grow relatively faster than the symmetric modes.

Our results from linear stability analyses confirm that the most unstable modes first appear in the month of May and last through the summer monsoon months. The growth rates and the amplitude structure of the most unstable modes agree reasonably with the time scale and structure of the meridional circulation during the monsoon transition. The main discrepancies of the modal eigenstructures are in predicting the latitudinal position of the vertical motions as compared to the observed structures found during the monsoon transition. These may presumably be attributed to the omission of the Hadley basic state as well as the lack of a realistic cumulus parameterization scheme. We are currently extending our analyses by incorporating all the basic states using a comprehensive model. However, in light of this present study, symmetric instability of zonal monsoon

flows may be a possible candidate for the sudden monsoon transition. More detailed modelling studies should be carried out to understand the physical connection between symmetric instability and the monsoon onset.

### 6. Acknowledgments

The authors are indebted to two anonymous reviewers who provided much constructive comments on the earlier version of the manuscript. We thank Dr. Y. C. Sud for discussions and also for reading the manuscript and making many helpful comments. The authors thank Mr. G. K. Walker for his assistance with the ECMWF data sets. One of the authors (VKK) is grateful to Prof. R. N. Keshavamurty, Director, Indian Institute of Tropical Meteorology, Pune and Dr. S. K. Mishra, Director, National Centre for Medium Range Weather Forecasting, New Delhi for many fruitful discussions. This work was performed while VKK held a National Research Council-(NASA) Research Associateship at the Goddard Space Flight Center, NASA.

### 7. Appendix

We simplify (11) by introducing discrete levels both in the vertical as well as the meridional direction and replacing the vertical and meridional derivatives by finite differences.

The finite differenced form of (11) at any interior grid point  $(J, K)$  is given by

$$\begin{aligned} & \frac{1}{\Delta p^2} \left( -f \left( f - \frac{\partial U}{\partial y} \right) \right) (\Psi_{J,K+1} - 2\Psi_{J,K} + \Psi_{J,K-1}) \\ & + \frac{1}{2\Delta p} \left( -\beta \frac{\partial U}{\partial p} \right) (\Psi_{J,K+1} - \Psi_{J,K-1}) \\ & + \frac{1}{2\Delta p 2\Delta y} \left( -2f \frac{\partial U}{\partial p} \right) \\ & \times (\Psi_{J+1,K+1} - \Psi_{J+1,K-1} - \Psi_{J-1,K+1} + \Psi_{J-1,K-1}) \\ & + \frac{1}{2\Delta y} \left( -f \frac{\partial^2 U}{\partial p^2} \right) (\Psi_{J+1,K} - \Psi_{J-1,K}) \\ & + \frac{1}{\Delta y^2} (-\sigma) (\Psi_{J+1,K} - 2\Psi_{J,K} + \Psi_{J-1,K}) \end{aligned}$$

$$\begin{aligned}
& + \frac{1}{2\Delta p \Delta y^2} \left( -\frac{K}{p} \sin\left(\frac{\pi p}{p_0}\right) \right) \\
& \times (-\Psi_{J+1,L-1} + 2\Psi_{J,L-1} - \Psi_{J-1,L-1}) - v^2 \\
& \times \left( \left( -\frac{1}{\Delta p^2} \right) (\Psi_{J,K+1} - 2\Psi_{J,K} + \Psi_{J,K-1}) \right) = 0.
\end{aligned} \tag{1}$$

Here  $f$  and  $\beta = \partial f / \partial y$  are functions of latitude and are evaluated at all latitude grid points. The vertical and lateral boundary conditions used are

$$\begin{aligned}
v &= -\frac{\partial \Psi}{\partial p} = 0; \quad \Psi|_{\pm y} = \text{constant} = 0, \\
\omega &= \frac{\partial \Psi}{\partial y} = 0; \quad \Psi \Big|_{\substack{p=0 \\ p=1000 \text{ mb}}} = \text{constant} = 0,
\end{aligned}$$

where  $+Y$  and  $-Y$  are the northern ( $42^\circ\text{N}$ ) and southern ( $42^\circ\text{S}$ ) boundaries respectively. Eq. (1) with the boundary conditions, (2) applied at latitudes  $J = 1, 2, \dots, N-1, N$  ( $40^\circ\text{S}, 38^\circ\text{S}, \dots, 38^\circ\text{N}, 40^\circ\text{N}$ ) and pressure levels  $K = 1, 2, \dots, L-1, L$  (100 mb, 200 mb,  $\dots$ , 800 mb, 900 mb) together

can be put into the form

$$(\tilde{A} - v^2 \tilde{B}) \tilde{Z} = 0, \tag{3}$$

where  $\tilde{A}$  and  $\tilde{B}$  are real square matrices of size ( $369 \times 369$ ),  $v^2$  is the eigenvalue and  $\tilde{Z}$  is the eigenfunction. The eigenfunction

$$\tilde{Z} = (\Psi_{1,1}, \Psi_{2,1}, \dots, \Psi_{N,1}, \Psi_{1,2}, \Psi_{2,2}, \dots, \Psi_{N-2}, \dots, \Psi_{1,L}, \Psi_{2,L}, \dots, \Psi_{N,L})^T, \tag{4}$$

the superscript  $T$  stands for the transpose. The coefficients of the matrices  $\tilde{A}$  and  $\tilde{B}$  are simple and hence will not be provided. Eq. (3) is a generalized eigenvalue problem and we have solved this equation with ( $K \neq 0$  in (1)) and without ( $K = 0$  in (1)) cumulus heating. The eigenvalues and eigenvectors are computed using the standard EISPACK eigensystem package (Smith et al., 1974). Physical modes were separated from numerical modes based on the absolute size of the parameters (which contain the information of eigenvalues) as the original matrix elements and also on the basis of spatial structures of eigenfunctions. The performance index calculation described therein, which gives the combined performance of all eigenvalues and corresponding eigenfunctions showed stable results.

#### REFERENCES

- Bennetts, D.A. and Hoskins, B. J. 1979. Conditional symmetrical instability—a possible explanation for frontal rainbands. *Quart. J. Roy. Meteor. Soc.* **105**, 945–962.
- Boyd, J. P. and Christidis, Z. D. 1982. Low wavenumber instability on the equatorial beta-plane. *Geophys. Res. Lett.* **9**, 769–772.
- Charney, J. G. 1973. Planetary fluid dynamics. *Dynamic meteorology*. Lecture Delivered at the Summer School of Space Physics of the Centre National d'etudes Spatiales, Lammion, France, P. Morel, Ed., D. Reidel, 622 pp.
- Dunkerton, T. J. 1981. On the inertial stability of the equatorial middle atmosphere. *J. Atmos. Sci.* **38**, 2354–2364.
- Dunkerton, T. J. 1993. Inertial instability of nonparallel flow on an equatorial  $\beta$  plane. *J. Atmos. Sci.* **50**, 2744–2758.
- Eliassen, A. 1952. Slow thermally or frictionally controlled meridional circulation in a circular vortex. *Astrophys. Norv.* **5**, 60.
- Emanuel, K. A. 1979. Inertial instability and mesoscale convective systems. Part I: Linear theory of inertial instability in rotating viscous fluids, *J. Atmos. Sci.* **36**, 2425–2449.
- Geisler, J. E. and Stevens, D. E. 1982. On the vertical structure of damped steady circulation in the tropics. *Quart. J. Roy. Meteor. Soc.* **108**, 87–93.
- Goswami, B. N., Shukla, J., Schneider, E. K. and Sud, Y. C. 1984. Study of the dynamics of the intertropical convergence zone with a symmetric version of the GLAS climate model. *J. Atmos. Sci.* **41**, 5–19.
- Held, I. M. and Hou, A. Y. 1980. Nonlinear axially symmetric circulations in a nearly inviscid atmosphere. *J. Atmos. Sci.* **37**, 515–533.
- Hoskins, B. J. 1974. The role of potential vorticity in symmetric stability and instability. *Quart. J. Roy. Meteor. Soc.* **100**, 480–482.
- Keshavamurty, R. N., Kasture, S. V. and Krishnakumar, V. 1986. 30–50 day oscillation of the monsoon: A new theory. *Beitr. Phys. Atmos.* **59**, 443–454.
- Krishnakumar, V. and Keshavamurty, R. N. 1993. Symmetric instability of monsoon zonal flows. *Atmósfera* **6**, 135–144.
- Kuo, H.-L. 1954. Symmetric disturbances in a thin layer of fluid subject to a horizontal temperature gradient and rotation. *J. Meteor.* **11**, 399–411.
- Lau, K. M. 1992. East Asian summer monsoon rainfall variability and climate teleconnection. *J. Meteor. Soc. Japan* **70**, 211–242.

- Lau, K. M. and L. Peng, 1987. Origin of low frequency (intraseasonal) oscillation in the tropical atmosphere. Part I: Basic Theory. *J. Atmos. Sci.* **44**, 950–972.
- Lau, K. M. and Yang, S. 1996. Seasonal variation, abrupt transition and intraseasonal variability associated with the Asian summer monsoon in the GLA GCM. *J. Climate* **9**, 965–985.
- Lau, K. M. and Li, M. T. 1984. The monsoon of east Asia and its global association – a survey. *Bull. Amer. Meteor. Soc.* **65**, 114–125.
- Lau, K. M., Yang, G. and Shen, S. H. 1988. Seasonal and intraseasonal climatology of summer monsoon rainfall over East Asia. *Mon. Wea. Rev.* **116**, 18–37.
- Mak, M. 1981. An inquiry into the nature of CISK. Part I. *Tellus* **33**, 531–537.
- Matsuno, T. 1966. Quasi-geostrophic motions in the equatorial area. *J. Meteor. Soc. Japan* **44**, 25–43.
- Ooyama, K. 1966. On the stability of the baroclinic circular vortex: A sufficient condition for instability. *J. Atmos. Sci.* **23**, 43–53.
- Plumb, R. A. and Hou, A. Y. 1992. The response of a zonally symmetric atmosphere to subtropical thermal forcing: Threshold Behavior. *J. Atmos. Sci.* **49**, 1790–1799.
- Schaack, T. K., Johnson, D. R. and Wei, M. Y. 1990. The three-dimensional distribution of atmospheric heating during the GWE. *Tellus* **42**, 305–327.
- Schneider, E. K. and Lindzen, R. S. 1976. A discussion of the parameterization of momentum exchange by cumulus convection. *J. Geophys. Res.* **81**, 3158–3160.
- Schubert, W. H. and Hack, J. J. 1982. Inertial stability and tropical cyclone development. *J. Atmos. Sci.* **39**, 1687–1697.
- Sikka, D. R. and Gadgil, S. 1980. On the maximum cloud zone and the ITCZ over India longitude during southwest monsoon. *Mon. Wea. Rev.* **108**, 1840–1853.
- Smith, B. T., Boyle, J. M., Garbow, B. S., Ikebe, Y., Klema, V. C. and Moler, C. B. 1974. Lecture notes in computer science, *Matrix eigensystem routines EISPACK Guide*, Springer-Verlag, New York.
- Stevens, D. E. 1983. On symmetric stability and instability of zonal mean flow near the equator. *J. Atmos. Sci.* **40**, 882–893.
- Stevens, D. E. and Ciesielski, P. E. 1986. Inertial instability of horizontally sheared flow away from the equator. *J. Atmos. Sci.* **43**, 2845–2856.
- Stone, P. H. 1966. On non-geostrophic baroclinic stability. *J. Atmos. Sci.* **23**, 390–400.
- Sun, W. Y. 1984. Rainbands and symmetric instability. *J. Atmos. Sci.* **41**, 3412–3426.
- Xu, Q. 1986. Conditional symmetric instability and mesoscale rainbands. *Quart. J. Roy. Meteor. Soc.* **112**, 315–334.
- Young, J. A. 1981. Low-level summer monsoon circulations. *Proceedings of the International Conference on Early results of FGGE and large-scale aspects of its monsoon experiments*. Tallahassee, **5.4–5.11**, Geneva, Switzerland.
- Zhang, D.-L. and Cho, H.-R. 1995. Three-dimensional simulation of frontal rainbands and conditional symmetric instability in the Eady-wave model. *Tellus* **47A**, 45–61.